IEEE Access
Multidisciplinary | Rapid Review | Open Access Journal

Received December 19, 2018, accepted January 6, 2019, date of publication January 22, 2019, date of current version February 8, 2019.

Digital Object Identifier 10.1109/ACCESS.2019.2894128

Detection of Neural Activity of Brain Functional Site Based on Microwave Scattering Principle

JING-KE WANG, XING JIANG, LIN PENG, (Member, IEEE), XIAO-MING LI, HONG-JIN AN, AND BAO-JIAN WEN

Department of Information and Communication, Guilin University of Electronic Technology, Guilin 541004, China

Corresponding authors: Xing Jiang (jiang_x@guet.edu.cn) and Lin Peng (penglin@guet.edu.cn)

This work was supported in part by the National Natural Science Foundation of China under Grant 61761012 and Grant 61371056, and in part by the Science and Technology Planning Project of Guangxi Province under Grant AB16380316.

ABSTRACT A method of detecting brain neural activity with the microwave transmission technology is presented in this paper. This method is based on the fact that the dielectric properties of brain functional site vary with the electrophysiological neural activity. The analysis of the uniform plane wave propagation of dynamic layered medium shows that the phase change of transmission coefficient (S-parameters) is consistent with the variation frequency of permittivity in the dynamic dielectric layer. A 3D head model was introduced to assign dynamic dielectric properties to the cerebral cortex by embedding a tissue piece in this head model. A six-element horn antenna array around the head model was designed, and two types of brain activity at various locations (visual cortex and auditory cortex) inside the head model has been discussed. The simulation results of microwave scattering in different directions show that forward scattering has better applicability. The frequency of the permittivity variation associated with the brain neuronal activity (10 Hz, 20 Hz) can be extracted from the phase variation on S-parameters. In addition, the specific absorption rate analysis ensures the safety of using the microwave in the design of human head detection systems.

INDEX TERMS Microwave transmission, dynamic dielectric, phase detection, SAR analysis.

I. INTRODUCTION

The detection and imaging of neuronal activities in brain has tremendous applications. Several techniques have been developed for such applications, including Electro- encephalography (EEG), Magnetoencephalography (MEG), functional magnetic resonance imaging (fMRI), opto-encephalography (OEG) and Intersectional Short Pulse (ISP) [1]–[4]. However, some of these applications involve ionizing radiation exposure and some are invasive detection methods. In recent years, microwave detection technology has emerged as a promising modality [5], [6]. An available approach has been provided by adopting microwave technology of head imaging to detect brain injuries and differentiate hemorrhagic from ischemic stroke in acute stroke patients [7]–[9]. In addition, different strategies have been developed for the modulation of brain function by non-invasive electrical stimulation [10], [11]. In similar concepts, microwave-based radiometry has been studied for dielectric measurement and temperature monitoring of biological tissues, the multi-frequency microwave radiometer provides an accurate and sensitive estimate for clinical monitoring of deep brain temperature profile [12], [13]. Recently, the application of microwave in detection of neuronal activity has been implemented [14]. These studies provide the possibility of detecting brain activity by using microwave technology.

In this paper, a microwave transmission method is proposed, which is based on the dynamic properties of dielectric at the brain functional site, to detect brain activity. It is a non-invasive strategy for brain neural activity at depth. The phase of the electromagnetic wave propagating through the brain functional site varies with the dynamic dielectric, and the frequency of the dielectric permittivity variation can be extracted from the phase variation of transmission coefficient.

II. THE RELATION OF FIELD QUANTITY IN LAYERED DYNAMIC MEDIUM

Electric fields generated by the neuron itself or applied externally can affect the transmembrane potential of the neuron, and consequently affect the probability of occurrence of action potential [15], [16]. The extracellular fluid surrounding the neurons at functional site in the brain is a typical dielectric of ionic polarization [17]. The permittivity of the dielectric

varies with the ion concentration of the extracellular fluid surrounding neurons in activation when the brainwaves are generated [18]. To deduce the relation between the transmission phase of electromagnetic wave and the dynamic dielectric properties, a three-layer simplified plane transmission model is adopted. The intermediate layer is a dynamic dielectric ($\varepsilon_2(t), \sigma, \mu_0$) which complex permittivity $\varepsilon_2(t)$ varies with time and the permeability is μ_0. For the convenience of research, the conductivity σ is set to a constant. Both sides are ordinary lossy media ($\varepsilon_1, \sigma, \mu_0$) with the same electrical parameters as shown in Fig. 1.

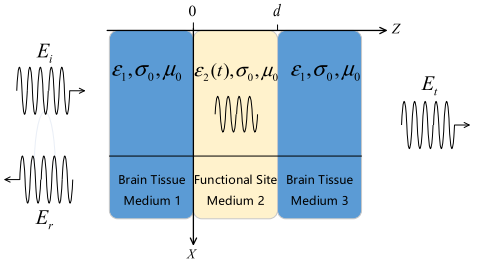

FIGURE 1. Three-layer medium transmission model.

Uniform plane wave can be decomposed into the superposition of TE wave and TM wave. Consider the TE wave normally incident from medium 1 through a plane boundary into medium 2. The fields of incident waves in medium 1 are given by [19]

$$\boldsymbol{E_{1i}}(z) = \vec{y}E_{1m}e^{-jk_1 z} \tag{1}$$

$$\boldsymbol{H_{1i}}(x) = -\vec{x}\frac{1}{\eta_1}E_{1m}e^{-jk_1 z} \tag{2}$$

where $k_1 = \omega\sqrt{\varepsilon_1\mu_0} = \omega\sqrt{(\varepsilon_0 \cdot \varepsilon_r - j\sigma/\omega)\mu_0}$ denote the propagation constant of plane wave in media 1, $\eta_1 = \sqrt{\mu_0}/\varepsilon_1$ denote the wave impedances of media 1; $\varepsilon_1 = \varepsilon_0 \cdot \varepsilon_r - j\sigma/\omega$ denote the complex permittivity; ε_0 denote the dielectric constant in vacuum; ε_r denote the relative permittivity; $\omega = 2\pi f_0$, and f_0 (3 GHz) denote the operating frequency.

The composed fields in medium 1 are given by the combination of the incident and the reflected files, and $z = 0$ is selected as the reference plane

$$\begin{aligned}\boldsymbol{E_1}(z) &= \boldsymbol{E_{1i}}(z) + \boldsymbol{E_{1r}}(z)\\ &= \vec{y}E_{1m}(e^{-jk_1 z} + R_{12}e^{jk_1 z})\end{aligned} \tag{3}$$

$$\begin{aligned}\boldsymbol{H_1}(z) &= \boldsymbol{H_{1i}}(z) + \boldsymbol{H_{1r}}(z)\\ &= -\vec{x}\frac{1}{\eta_1}E_{1m}(e^{-jk_1 z} - R_{12}e^{jk_1 z})\end{aligned} \tag{4}$$

where R_{12} is the reflection coefficient of the interface.

In medium 2, $z = d$ is selected as the reference plane and the composed fields is

$$\begin{aligned}\boldsymbol{E_2}(z) &= \vec{y}E_{2m}(e^{-jk_2(z-d)} + R_{23}e^{jk_2(z-d)})\\ &= \vec{y}T_{12}E_{1m}(e^{-jk_2(z-d)} + R_{23}e^{jk_2(z-d)})\end{aligned} \tag{5}$$

$$\boldsymbol{H_2}(z) = -\vec{x}\frac{1}{\eta_2}T_{12}E_{1m}(e^{-jk_2(z-d)} - R_{23}e^{jk_2(z-d)}) \tag{6}$$

where R_{23} is the reflection coefficient of the interface $z = d$, $T_{12}e^{jk_2 d}$ is the transmission coefficient of the interface $z = 0$.

As a functional brain site has activity, the activation of the neurons (synchronised at a frequency) periodically varies the ion concentration in the volume of the extracellular fluid and the permittivity of the medium varies correspondingly [18]. Therefore, we added periodic rhythmic changes to the average permittivity of the brain tissue ($\varepsilon_r = 48$ at 3 GHz). The complex permittivity $\varepsilon_2(t) = \varepsilon_0 \cdot \varepsilon_r(t) - j\sigma/\omega$ in the medium 2 is a time-variant parameter, and its expression is set as follows

$$\varepsilon_r(t) = 48 + 3\sin(2\pi f_i t) \tag{7}$$

where 48 is the average relative permittivity of brain tissue at 3 GHz, f_i (5 Hz, 15 Hz) denote the frequency of permittivity variation of the dynamic dielectric; $k_2 = \omega\sqrt{(\varepsilon_0 \cdot \varepsilon_r(t) - j\sigma/\omega)\mu_0}$ denote the propagation constant in medium 2; $\eta_2 = \sqrt{\mu_0}/\varepsilon_2(t)$ denote the wave impedances of media 2.

The fields in medium 3 are transmitted fields only, $z = d$ is selected as the reference plane

$$\boldsymbol{E_3}(z) = \vec{y}E_{3m}e^{-jk_3(z-d)} = \vec{y}T_{12}T_{23}E_{1m}e^{-jk_3(z-d)} \tag{8}$$

$$\boldsymbol{H_3}(z) = -\vec{x}\frac{1}{\eta_3}T_{12}T_{23}E_{1m}e^{-jk_3(z-d)} \tag{9}$$

where T_{23} is the transmission coefficient of the interface $z = d$. As the media on both sides are the same, we have the propagation constant $k_3 = k_1$, and the wave impedances $\eta_3 = \eta_1$.

On the boundary of the two media, both the tangential component of the composed electric field and the tangential component of the composed magnetic fields must be continuous at the boundary $z = d$. The boundary equations are given by

$$n \times \boldsymbol{E_2}|_{z=d} = n \times \boldsymbol{E_3}|_{z=d}\ ,\ \text{i.e. } 1 + R_{23} = T_{23} \tag{10}$$

$$n \times \boldsymbol{H_2}|_{z=d} = n \times \boldsymbol{H_3}|_{z=d}\ ,\ \text{i.e. } \frac{1}{\eta_2}(1 - R_{23}) = \frac{1}{\eta_3}T_{23} \tag{11}$$

from (10) and (11), we get

$$R_{23}(t) = \frac{\eta_3 - \eta_2}{\eta_3 + \eta_2}, \quad T_{23}(t) = \frac{2\eta_3}{\eta_3 + \eta_2} \tag{12}$$

Similarly, at the boundary of the medium 1 and the medium 2, we get

$$\begin{aligned}R_{12}(t,d) &= \frac{\eta_d - \eta_1}{\eta_d + \eta_1}, \quad \eta_d = \eta_2\frac{\eta_3 + j\eta_2\tan(k_2 d)}{\eta_2 + j\eta_3\tan(k_2 d)}\\ T_{12}(t,d) &= \frac{1 + R_{12}}{e^{jk_2 d} + R_{23}e^{-jk_2 d}}\end{aligned} \tag{13}$$

where η_d denote the equivalent wave impedance at $z = 0$.

Aiming at the influence of the dynamic dielectric layer on the transmission process, the reflection coefficient is defined as

$$S_{11} = \frac{\boldsymbol{E_r}}{\boldsymbol{E_i}} = R_{12}(t,d) = |S_{11}| \cdot e^{j\varphi_r} \tag{14}$$

The transmission coefficient is defined as

$$S_{21} = \frac{\boldsymbol{E_t}}{\boldsymbol{E_i}} = T_{12}(t, d) \cdot T_{23}(t) = |S_{21}| \cdot e^{j\varphi_t} \tag{15}$$

The transmitted and backscattered signals are calculated by finding out the solution of the above equations using the Matlab programming. For the limited range of $\varepsilon_2(t)$, the relationship between $\varepsilon_2(t)$ and transmission phase-φ can be expressed as ($d = 2$cm)

$$\varphi_r = f[\varepsilon_2(t), d] \tag{16}$$

where φ_r is a complex function of $\varepsilon_2(t)$ and d.

Similarly, S_{21} can be approximated as

$$S_{21} = \frac{1 + R_{12}}{e^{jk_2 d} + R_{23}e^{-jk_2 d}} \cdot \frac{2\eta_3}{\eta_3 + \eta_2} \frac{R_{12} \ll 1, \eta_3 \approx \eta_2}{R_{23}e^{-jk_2 d} \ll e^{jk_2 d}} \Rightarrow e^{-jk_2 d} \tag{17}$$

where φ_t can be rewritten as $-\mathrm{Re}\{k_2\}d$

The amplitude of the transmitted phase within 1s is defined as

$$\text{Forward scattered: } |\varphi_t| = \max\{\varphi_t\} - \min\{\varphi_t\} \tag{18}$$

$$\text{Backscattered: } |\varphi_r| = \max\{\varphi_r\} - \min\{\varphi_r\} \tag{19}$$

According to the above analysis, the phase φ_r of reflection coefficient S_{11} and the phase φ_t of transmission coefficient S_{21} can be expressed as a function of complex permittivity $\varepsilon_2(t)$ and thickness d. Moreover, since a single-frequency microwave transmission method is adopted in this work, the frequency dependency is neglected in the analysis processes.

The cases of $f_i = 5$ Hz and $f_i = 15$ Hz are discussed. Fig. 2(a), (e) and 2(c), (g) show the time domain distribution of phase calculated by backscattered method and forward scattered method respectively. It is shown that the dynamic properties of the dielectric layer cause changes in the transmission phase. Fig. 2(b), (f) and 2(d), (h) show that the spectral curve has a peak which is equal to the frequency f_i of permittivity variation at the dynamic layer. The results show that there is a corresponding relationship between the transmission phase and the change of permittivity. That is, they have the same characteristic frequency.

Refer to (14),(15) and (17), it can be seen that φ_r presents fluctuation with the increase of dynamic layer thickness which affected by the *tan*-function and η_d, and φ_t affected by exponential factor $-jk_2 d$ increases linearly with dynamic layer thickness. Fig. 3 shows the effect of different thicknesses of dynamic dielectric layer and frequency on the phase of transmission which is consistent with the above analysis. The phase calculated by forward scattering method has a larger fluctuation range. Therefore, forward scattering is considered to have better performance and applicability. Simulation results also show that microwave operating at 3 GHz can effectively penetrate the brain and provide good spatial resolution.

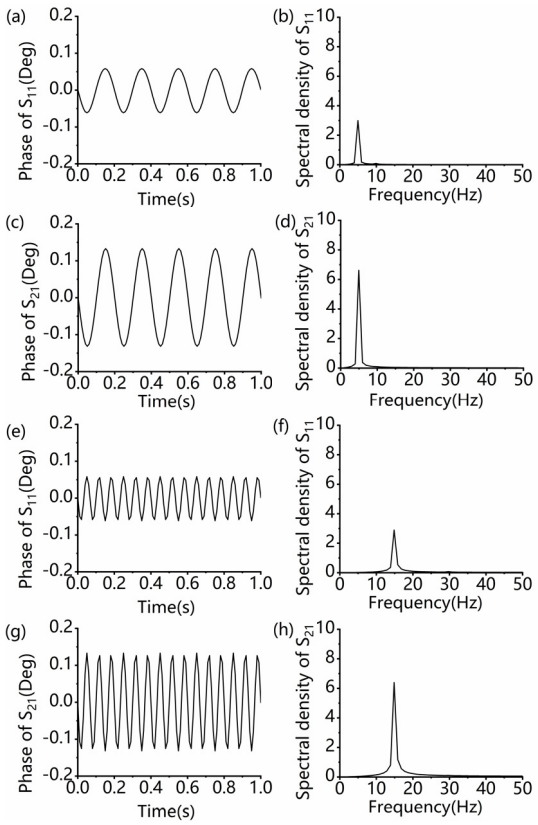

FIGURE 2. The transmission phase and spectrum of electromagnetic wave through three-layer dynamic medium. (a), (e) The phase φ_r variation of reflection coefficient S_{11} with mean processing. (b), (f) Spectrum density of φ_r with FFT. (c), (g) The phase φ_t variation of transmission coefficient S_{21} with mean processing. (d), (h) Spectrum density of φ_t with FFT.

III. METHODS AND RESULTS

In this section, the process on simulation is described and the performance of different microwave scattering methods are compared. We use a 3D human head model which is derived from software COMSOL Multiphysics (M. Levoy, MRI data originally from University of North Carolina). The original model is a homogeneous human head model consisting of a single material. Considering the complex physiological structure of the brain, a 2-layer model was constructed based on the original model, one of which is the skull and the rest is the brain tissue to avoid heavy computation tasks. This head model is assigned average dielectric properties of brain tissue.

A. SIMULATION OF BRAIN FUNCTION IN DIFFERENT POSITIONS IN HUMAN HEAD MODEL

The propagation characteristics of electromagnetic wave in dynamic media are simulated and verified in electromagnetic simulation software FEKO which is based on the method of moments (MoM). The MoM mesh setting for this example utilizing the integral equations method in the frequency domain is: number of triangles: 17656, mesh size: 0.02λ (cortex), 0.07λ (skull and brain tissue). Brainwaves are spontaneous rhythmic nerve electrical activities whose frequency

TABLE 1. The material properties of the head model [21].

Tissue	Electrical conductivity (S/m)	Relative permittivity
Skull	0.31	16
Brain tissue	2.2	48
Functional site	2.2	$48+3\sin(2\pi f_i t)$

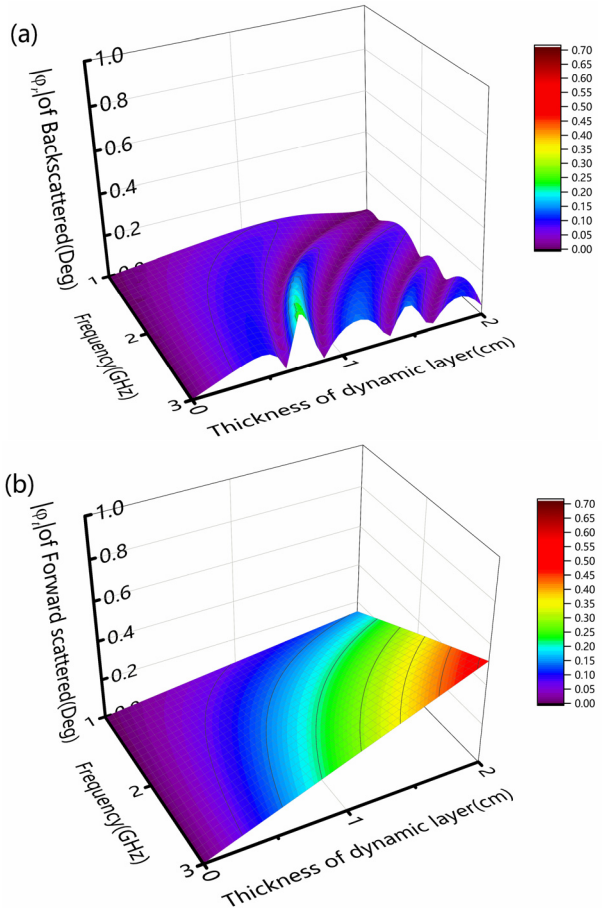

FIGURE 3. Effect of frequency (from 1 GHz to 3 GHz) and distance (from 0 cm to 2 cm) on transmission phase. (a) Backscattering method ($|\varphi_r|$ of S_{11}). (b) Forward scattering method ($|\varphi_t|$ of S_{21}).

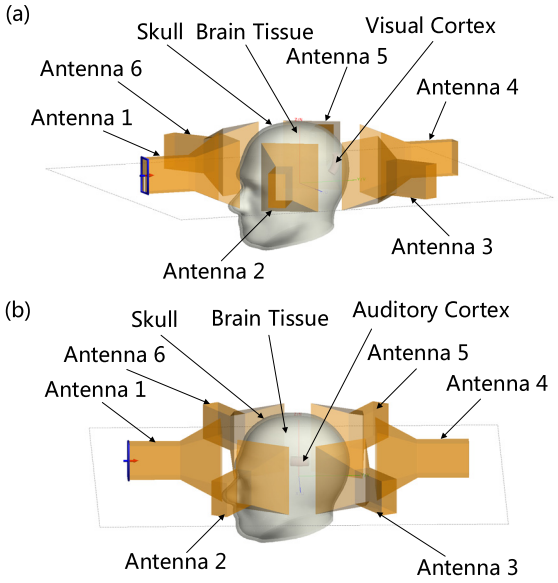

FIGURE 4. Simulation of neural activity in brain functional site at different locations. (a) Visual Cortex (b) Auditory Cortex.

varies from 1 to 30 times per second, and it can be divided into four bands, namely δ-wave (0.1-3 Hz), θ-wave (4-7 Hz), α-wave (8-12 Hz), β-wave (13-40 Hz) [20]. The relative permittivity of the dynamic dielectric (visual cortex $f_i = 20$ Hz, auditory cortex $f_i = 10$ Hz) in the brain functional site is $\varepsilon_r(t) = 48 + 3\sin(2\pi f_i t)$. Here, t is the duration of the change in permittivity, f_i represents the rhythm of neural activity in the brain functional site. The sampling time is set to 1 second and the step size is $t = 0.01$ seconds. As shown in Fig. 4, six-element horn antenna array are distributed around the head model with equal distance. Antenna 1 is used as the transmitter, and antenna 1, 2, 3, 4,5 and 6 are respectively used for receiving. The phase differences in scattered electric field signals at antenna locations are used to indicate the presence of brain activity. The characteristic frequency is extracted by FFT based on the amount of changes in the received S-parameters phase information. Here, the auditory cortex and the visual cortex are used as research objects. The material properties of the head model are shown in Table 1.

1) SIMULATION OF NEURAL ACTIVITY IN VISUAL CORTEX

The visual cortex of the brain is a part of the cerebral cortex that processes visual information. It is located in the occipital lobe. To emulate the neural activity of the visual cortex, a strip tissue with the dynamic dielectric properties is inserted inside the head model as shown in Fig. 4(a) [22]. The simulation results of phase variation in time domain and its spectrum distribution are shown in Fig. 5. Because of the difference of transmission path, the second harmonic component of backscattering is larger than its own characteristic frequency. However, forward scattering has a high concentration of spectrum. The spectrogram shows that the frequency of the phase change of the receiving antenna at different positions is concentrated at 20 Hz which is consistent with the characteristic frequency f_i of the permittivity variation of dynamic dielectric of the functional site. By comparing different scattering cases, the phase information received by antennas contains

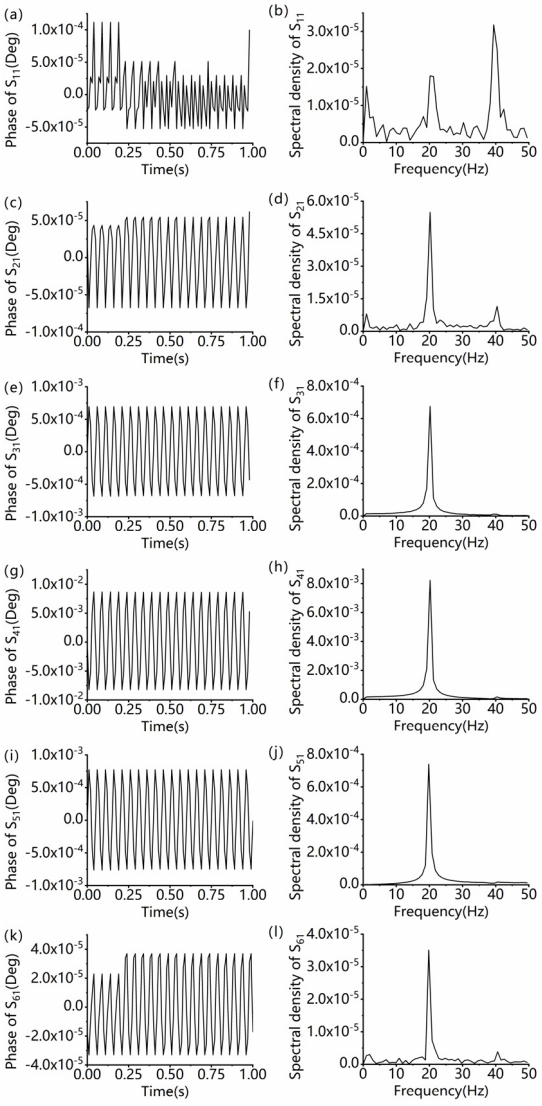

FIGURE 5. Simulation results of visual cortex in head model. (a), (c), (e), (g), (i), (k) represents the phase variation of the transmission coefficient of antenna 1-6 respectively. (b), (d), (f), (h), (j), (l) represents the corresponding spectral density distribution.

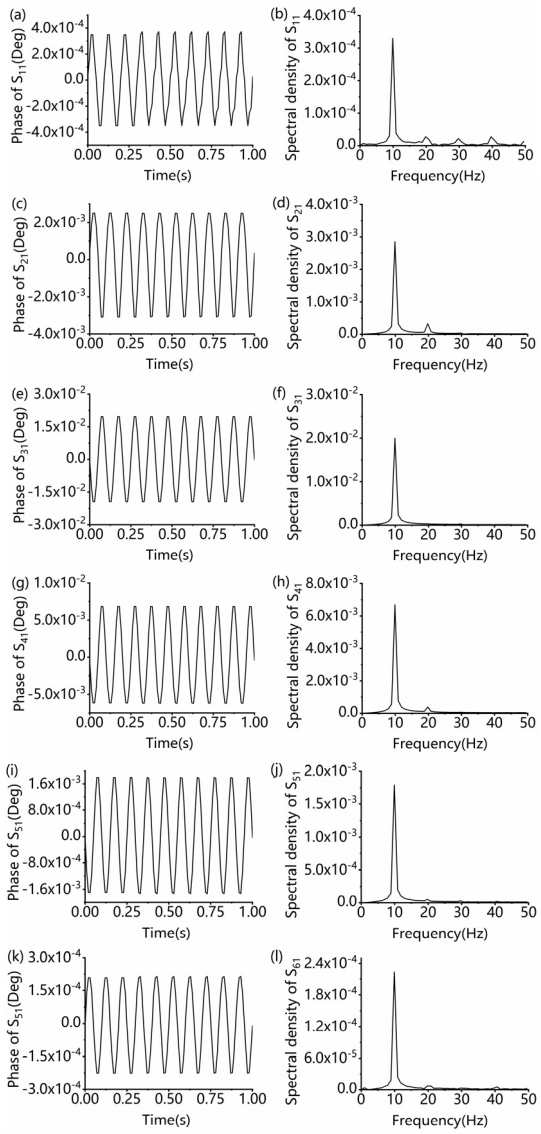

FIGURE 6. Simulation results of auditory cortex in head model. (a), (c), (e), (g), (i), (k) represents the phase variation of the transmission coefficient of antenna 1-6 respectively. (b), (d), (f), (h), (j), (l) represents the corresponding spectral density distribution.

higher harmonic and spurious frequencies. There is no linear relationship between the complex permittivity ε and the phase function φ.

The ranges of normalized phase change and spectrum evaluated at different receiving antennas of the visual cortex are provided in Table 2. The normalized phase of S_{41} varies from -8.216×10^{-3} to 8.636×10^{-3} degree over time with the highest spectral component at 20 Hz.

2) SIMULATION OF NEURAL ACTIVITY IN AUDITORY CORTEX

The auditory cortex is the part of the temporal lobe that processes auditory information in humans. It is located bilaterally, roughly at the upper sides of the temporal lobes as shown in Fig. 4(b) [22]. The simulation results of phase variation in time domain and frequency domain are shown in Fig. 6. There is a peak frequency at 10 Hz in the spectrum. It indicated that the neural activity in different locations can be detected by microwave transmission. The ranges of normalized phase change and spectrum evaluated at different receiving antennas of the auditory cortex are provided in Table 3. The normalized phase of S_{31} varies from -1.942×10^{-2} to 1.965×10^{-2} degree over time with the highest spectral component at 10 Hz. Therefore, forward scattering has better performance when the functional site is located between a set of transmit and receive antennas.

B. SPECIFIC ABSORPTION RATE ANALYSIS

Specific absorption rate (SAR) is a measure of the rate at which energy is absorbed by the human body when exposed to a radio frequency (RF) electromagnetic field. It is defined as the power absorbed per mass of tissue and has units of

TABLE 2. Phase information and spectrum distribution of visual cortex.

Number of antennas	Range of phase change (Deg)	Spectrum peak (at 20 Hz)
1	$-5.266 \times 10^{-5} \sim 1.117 \times 10^{-4}$	1.80×10^{-5}
2	$-6.751 \times 10^{-5} \sim 6.150 \times 10^{-5}$	5.49×10^{-5}
3	$-6.848 \times 10^{-4} \sim 6.952 \times 10^{-4}$	6.75×10^{-4}
4	$-8.216 \times 10^{-3} \sim 8.636 \times 10^{-3}$	8.23×10^{-3}
5	$-7.645 \times 10^{-4} \sim 7.745 \times 10^{-4}$	7.38×10^{-4}
6	$-3.302 \times 10^{-5} \sim 3.698 \times 10^{-5}$	3.51×10^{-5}

TABLE 3. Phase information and spectrum distribution of auditory cortex.

Number of antennas	Range of phase change (Deg)	Spectrum peak (at 10 Hz)
1	$-3.501 \times 10^{-4} \sim 3.719 \times 10^{-4}$	3.30×10^{-4}
2	$-3.090 \times 10^{-3} \sim 2.511 \times 10^{-3}$	2.86×10^{-3}
3	$-1.942 \times 10^{-2} \sim 1.965 \times 10^{-2}$	1.96×10^{-2}
4	$-6.209 \times 10^{-3} \sim 6.837 \times 10^{-3}$	6.68×10^{-3}
5	$-1.730 \times 10^{-3} \sim 1.795 \times 10^{-3}$	1.80×10^{-3}
6	$-2.252 \times 10^{-4} \sim 2.148 \times 10^{-4}$	2.24×10^{-4}

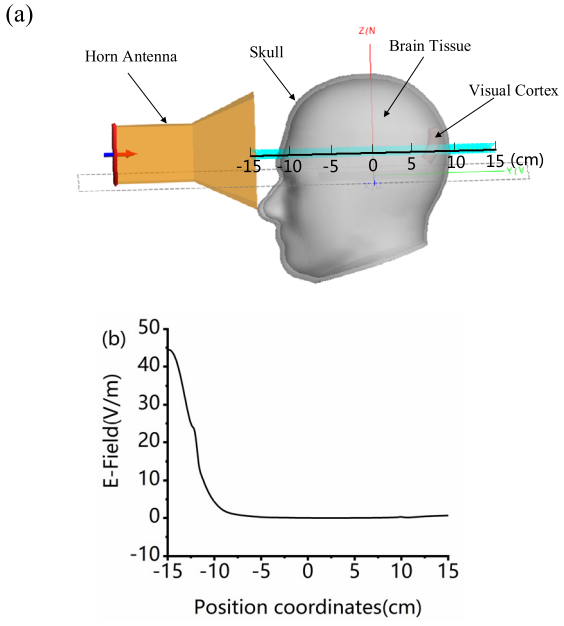

FIGURE 7. (a) SAR analysis in head model at 3 GHz. (b) Distribution of E-field on the reference line.

watts per kilogram. SAR for electromagnetic energy can be calculated from the electric field within the tissue as

$$\mathrm{SAR} = \frac{\sigma |E|^2}{2\rho} \tag{20}$$

where E denote the electric field, ρ express the density of body tissue.

According to the IEEE standard of safety levels (C95.1-2005) [23] and European Committee for Electrotechnical Standardization (CENELEC) for the RF energy emitted by mobile devices [24], an average SAR value below 2 W/kg over 10 g of tissue is reported as a safety limit. To examine the ionization effects of MW signals to a human head, we have selected No.1 of the above horn antenna array as the transmitting antenna, and operated at the 3 GHz frequency with 10 mW transmitted power. The peak SAR values of 0.108 W/kg were reported. Fig. 7(b) shows that the energy of the electric field is reduced from 44.34 V/m to 8.84 V/m at the skull (at −11cm on the reference line). It shows that most of the energy is reflected and absorbed by the skull near the antenna side. These values are far below the suggested limit, thus guaranteeing the safe usage of a microwave head-transmitting system.

IV. CONCLUSION

This study provides the application of microwave transmission technology in the detection of brain activity. The propagation of uniform plane wave in a three-layer dynamic medium demonstrates the relationship between the change of permittivity and the transmission phase. Simulations in a 3D head model suggests that brain activity at different locations can be indicated by the information of phase change obtained from the receiving antenna. The phase changes of S-parameters are consistent with the frequency of the dynamic permittivity in the activation area. Comparison analysis emphasizes that these differences vary with the type and location of brain activity.

REFERENCES

[1] T. Murta, M. Leite, D. W. Carmichael, P. Figueiredo, and L. Lemieux, "Electrophysiological correlates of the BOLD signal for EEG-informed fMRI," *Hum. Brain Mapping*, vol. 36, pp. 391–414, Jan. 2015.

[2] A. Ukil, "Denoising and frequency analysis of noninvasive magnetoencephalography sensor signals for functional brain mapping," *IEEE Sensors J.*, vol. 12, no. 3, pp. 447–455, Mar. 2012.
[3] O. Hiwaki1 and H. Miyaguchi, "Noninvasive measurement of dynamic brain signals using light penetrating the brain," *PLoS ONE*, vol. 13, no. 1, p. e0192095, Jan. 2018.
[4] M. Vöröslakos *et al.*, "Direct effects of transcranial electric stimulation on brain circuits in rats and humans," *Nature Commun.* vol. 9, p. 483, Feb. 2018.
[5] J. Sachs, S. Ley, T. Just, S. Chamaani, and M. Helbig, "Differential ultra-wideband microwave imaging: Principle application challenges," *Sensors*, vol. 18, no. 7, p. 2136, Jul. 2018.
[6] H. Hinrikus, M. Bachmann, and J. Lass, "Effect of 7, 14 and 21 Hz modulated 450 MHz microwave radiation on human electroencephalographic rhythms," *Int. J. Radiat. Biol.*, vol. 84, no. 1, pp. 69–79, Jan. 2008.
[7] S. Mustafa, B. Mohammed, and A. Abbosh, "Novel preprocessing techniques for accurate microwave imaging of human brain," *IEEE Antennas Wireless Propag. Lett.*, vol. 12, pp. 460–463, Mar. 2013.
[8] M. Hopfer, R. Planas, A. Hamidipour, T. Henriksson, and S. Semenov, "Electromagnetic tomography for detection, differentiation, and monitoring of brain stroke: A virtual data and human head phantom study," *IEEE Antennas Propag. Mag.*, vol. 59, no. 5, pp. 86–97, Oct. 2017.
[9] A. M. Qureshi, Z. Mustansar, and S. Mustafa, "Finite-element analysis of microwave scattering from a three-dimensional human head model for brain stroke detection," *Roy. Soc. Open Sci.*, vol. 5, p. 180319, Jun. 2018.
[10] N. Grossman *et al.*, "Noninvasive deep brain stimulation via temporally interfering electric fields," *Cell*, vol. 169, pp. 1029–1041, Jun. 2017.
[11] M. H. Histed, V. Bonin, and R. C. Reid, "Direct activation of sparse, distributed populations of cortical neurons by electrical microstimulation," *Neuron*, vol. 63, no. 4, pp. 508–522, Aug. 2009.
[12] P. Wang and C. L. Brace, "Tissue dielectric measurement using an interstitial dipole antenna," *IEEE Trans. Bio-Med. Eng.*, vol. 59, no. 1, pp. 115–121, Jan. 2012.
[13] K. Maruyma *et al.*, "Feasibility of noninvasive measurement of deep brain temperature in newborn infants by multifrequency microwave radiometry," *IEEE Trans. Microw. Theory Techn.*, vol. 48, no. 11, pp. 2141–2147, Nov. 2000.
[14] X. Jiang, Z. Geng, X. Li, L. Peng, B. Kang, and C. Zheng, "Microwave transmission approach for dynamic dielectric detection at brain functional site," in *IEEE MTT-S Int. Microw. Symp. Dig.*, Jun. 2017, pp. 1235–1238.
[15] C. A. Anastassiou, S. M. Montgomery, M. Barahona, G. Buzsáki, and C. Koch, "The effect of spatially inhomogeneous extracellular electric fields on neurons," *J. Neurosci.*, vol. 30, no. 5, pp. 1925–1936, Feb. 2010.
[16] H. R. Heekeren, S. Marrett, and L. G. Ungerleider, "The neural systems that mediate human perceptual decision making," *Nature Rev. Neurosci.*, vol. 9, pp. 467–479, Jun. 2008.
[17] P. Somogyi and T. Klausberger, "Defined types of cortical interneurone structure space and spike timing in the hippocampus," *J. Physiol.*, vol. 562, no. 1, pp. 9–26, Jan. 2005.
[18] X. P. Li *et al.*, "The dynamic dielectric at a brain functional site and an EM wave approach to functional brain imaging," *Sci. Rep.*, vol. 4, p. 6893, Nov. 2014.
[19] K. Q. Zhang and D. J. Li, "Introduction to wave," in *Electromagnetic Theory for Microwaves and Optoelectronics*, 2nd ed. Berlin, Germany: Springer, 2008, pp. 80–83.
[20] F. R. On, R. Jailani, H. Norhazman, and N. M. Zaini, "Binaural beat effect on brainwaves based on EEG," in *Proc. IEEE 9th Int. Colloq. Signal Process. Appl.*, Jun. 2013, pp. 339–343.
[21] IFAC. *Dielectric Properties of Body Tissues[DB/OL]*. [Online]. Available: https://niremf.ifac.cnr.it/tissprop/htmlclie/htmlclie.php
[22] Wikipedia Contributors. *Cerebral Cortex*. Accessed: Sep. 9, 2018. [Online]. Available: https://en.wikipedia.org/w/index.php?title=Cerebral_cortex&oldid=852423695
[23] *IEEE Standard for Safety Levels With Respect to Human Exposure to Radio Frequency Electromagnetic Fields, 3 kHz to 300 GHz*, IEEE Standard C95.1-2005 (Revision of IEEE Standard C95.1-1991), Apr. 2006, pp. 1–238.
[24] *TC 106—Methods for the Assessment of Electric, Magnetic and Electromagnetic Fields Associated With Human Exposure*, IEC Standard 62209-1, Feb. 2005.

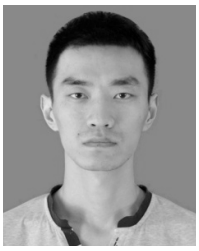

JING-KE WANG was born in Henan, China, in 1991. He received the B.E. degree in computer science and technology from Zhengzhou University, Henan, in 2014. He is currently pursuing the master's degree with the Guilin University of Electronic Technology. His research interests include antennas and biological electromagnetics.

XING JIANG received the master's degree in electromagnetic field and microwave technology from the Beijing Institute of Technology, in 1986. Since 2000, she has been with the Guilin University of Electronic Technology as a Professor. She has published over 30 papers. Her research interests include smart communication system design, conformal antenna array, and bioelectromagnetics. She is sponsored by the National Natural Science Foundation of China and the Natural Science Foundation of Guangxi. She is a Senior Member of the China Communications Society and a member of the Chinese Institute of Electronics.

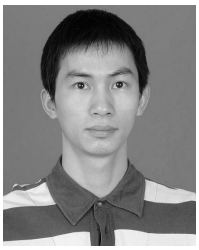

LIN PENG (M'16) was born in Guangxi, China, in 1981. He received the B.E. degree in science and technology of electronic information, and the master's and Ph.D. degrees in radio physics from the University of Electronic Science and Technology of China, Chengdu, China, in 2005, 2008, and 2013, respectively.

Since 2013, he has been with the Guilin University of Electronic Technology, where he became an Associate Professor, in 2016. From 2011 to 2013, he was sponsored by the China Scholarship Council to study from the University of Houston as a joint Ph.D. Student. He has published over 30 papers as the first and corresponding author. He has co-authored over 20 papers. His research interests include terahertz technologies, metamaterials, antenna/filter theory and design, electromagnetic bandgap structure design and its application in antenna, composite right/left-handed transmission line and its applications, and conformal antenna array.

In recent years, he is sponsored by several funds, such as the Fundamental Research Funds for the Central Universities, the National Natural Science Foundation of China, the Natural Science Foundation of Guangxi, the Program for Innovative Research Team of the Guilin University of Electronic Technology, and the Guangxi Key Laboratory of Wireless Broadband Communication and Signal Processing. He serves as an Associate Editor for the IEEE Access. He also serves as a Reviewer for the IEEE Transactions on Microwave Theory and Techniques, the IEEE Transactions on Antennas and Propagation, the IEEE Microwave and Wireless Components Letters, the IEEE Antennas and Wireless Propagation Letters, *Electronics Letters*, the IET Microwave, Antennas & Propagation, the *IET Communications*, *Wireless Personal Communications*, *Progress in Electromagnetics Research*, and the *Journal of Electromagnetic Waves and Applications*.

XIAO-MING LI was born in Shandong, China, in 1979. He received the B.E. and master's degrees from the Guilin University of Electronic Technology, Guilin, China, in 2002 and 2005, respectively, where he is currently a Lecturer. His research interests include antennas and electromagnetic measurements.

HONG-JIN AN was born in Sichuan, China, in 1992. She received the B.E. degree in electronic information engineering from Jinjiang College, Sichuan, in 2015. She is currently pursuing the master's degree with the Guilin University of Electronic Technology. Her research interests include antennas and biological electromagnetics.

BAO-JIAN WEN was born in Guangxi, China, in 1989. He received the B.E. degree in communication engineering from the Chengdu University of Information Technology, Sichuan, China, in 2015. He is currently pursuing the master's degree with the Guilin University of Electronic Technology. His research interests include antennas and metamaterials.